Applied Thermal Engineering 39 (2012) 78–85

Contents lists available at SciVerse ScienceDirect

Applied Thermal Engineering

journal homepage: www.elsevier.com/locate/apthermeng

A new method of defrosting evaporator coils

G. Mader*, C. Thybo

Danfoss A/S, Thermodynamics & Product Concepts, Nordborgvej 81, 6430 Nordborg, Denmark

ARTICLE INFO

Article history:
Received 29 September 2011
Accepted 13 January 2012
Available online 28 January 2012

Keywords:
Heat pump
Defrost
Expansion valve
Energy efficiency
Microchannel heat exchanger

ABSTRACT

A new method is presented to defrost evaporator coils of heat pumps using air as a heat source. At low outdoor temperatures the evaporation temperature can drop below the freezing point of water, the water vapor in the air then freezes on the outer surface of the coil. This increases air side pressure drop and reduces the heat transfer capability of the evaporator coil, leading to a decrease in system efficiency. Long frost build-up times would lead to a partly or totally blocked evaporator coil, rendering the system inoperable. To maintain the functionality of the system it is therefore necessary to remove the frost regularly. For a reversible air conditioning system this is typically done by reversing the flow of the system. In the reversed mode the outdoor coil serves as a condenser, hereby melting the frost on the coil surface. Each of these defrost cycles however further reduces the system efficiency substantially. The new method uses an actively distributing valve which is able to feed parallel evaporator passes individually. With this valve single evaporator circuits are regularly shut off. While no refrigerant is evaporated in a closed circuit, the coil surface temperature increases and the flow of the ambient air is sufficient to defrost this part of the evaporator as long as the air temperature is above 0 °C. Experimental results show that under standard frost conditions the evaporator can be kept frost-free and even under severe conditions most of the highly inefficient system reversals can be avoided. Thereby system efficiency is increased significantly.

1. Introduction

1.1. Frost growth

A vapor compression heat pump absorbs heat from the ambient on a low temperature level and transfers it to a high temperature level where the heat is rejected and used e.g. for heating a house. For heat pumps using ambient air as heat source frost forms on the evaporator surface in operating conditions with low temperature and high humidity air and evaporator surface temperatures below the freezing point. A number of studies experimentally investigate the mechanisms and effects of frost growth on finned tube heat exchangers under varying operating conditions and evaporator geometries.

Air inlet temperature, relative humidity, air mass flow rate and evaporator surface temperatures are identified to strongly influence the frost formation. Lee and Kim [1] present both frost thickness after a constant time period and averaged energy transfer resistance as indicator for frost formation under varying air conditions. For increasing air temperatures between 4 °C and 10 °C and a constant humidity ratio both frost thickness and energy transfer resistance decrease continuously indicating that with higher temperatures thinner but denser frost layers are formed. With increasing relative humidities both frost thickness and energy transfer resistance increase indicating thicker, less dense frost formation. With increasing inlet air velocity however frost thickness increases while energy transfer resistance decreases indicating both thicker and denser frost layers. These observations are explained with the interaction of two different frost growth mechanisms: 1) frost growth at the surface which increases frost thickness and the insulating effect of the layer and is induced by high mass transfer and 2) vapor diffusing into the frost layer which increases frost density and thereby reduces the insulating effect. Tassou and Marquand [2] investigate the effects of frost formation on heating capacity and COP for air temperatures between 5 °C and −3 °C at a constant relative humidity of 60%. The degradation on both heating capacity and COP is found to be increasingly larger for higher air temperatures. Also increasing relative humidities at a constant air temperature are found to lead to faster degradations of capacity and efficiency. Votsis and Tassou [3] as well as Yan *et al.* [4] present the air pressure drop over the coil as an indication of the frost formation. Both keep relative humidities constant at 82% and

* Corresponding author.
E-mail address: gunda.mader@danfoss.com (G. Mader).

1359-4311/$ – see front matter © 2012 Elsevier Ltd. All rights reserved.
doi:10.1016/j.applthermaleng.2012.01.033

Nomenclature

Roman

A	area [m^2]
$\tilde{A}$	relative free cross flow area [−]
c_p	specific heat capacity at constant pressure [J/kg K]
d	thickness [m]
H_{fin}	fin height [m]
h	specific enthalpy [J/kg]
M	mass [kg]
$\dot{M}$	mass flow rate [kg/s]
P_{fin}	fin pitch [m]
$\dot{Q}$	heat transfer rate [W]
T	temperature [K]
$\dot{V}$	volume flow rate [m^3/s]
X	humidity ratio [$kg_{water}/kg_{dry\ air}$]

Greek

α	heat transfer coefficient [W/m^2 K]
β	mass transfer coefficient [m/s]
ρ	density [kg/m^3]

Subscripts

0	initial state
a	air
f	frost
f,s	sublimation
f,d	drainage
I	inlet
l	latent
O	outlet
r	refrigerant
S	surface
s	sensible
t	total

70% respectively while varying the air temperature. Both find a maximum in pressure drop increase [3], at 0 °C [4], at 5 °C. One reason for the different observations might be that different relative humidities are adjusted and that humidity ratios vary strongly with constant relative humidity for varying temperatures. Furthermore significantly different coolant temperatures are chosen in the different studies which also can contribute to the discrepancies.

These differences notwithstanding for a wide range of operating conditions a characteristic pattern for changes of capacity and COP with increasing frost growth can be described: During the initial frost growth period an increase in heat transfer rate and evaporator capacity might be observed, as reported among others by [1] and Guo *et al.* [5]. It is attributed to an increase in surface roughness and area while frost layers are not yet thick enough to have an insulating effect or block the free flow area. This effect can however not be seen in the results of Kondepudi and O'Neal [6] as well as those of Xia *et al.* [7]. Both investigate louvered fins, pointing out that frost blocks the louvers first thus destroying their positive area and turbulence enhancement effects which cannot be compensated by the frost roughness effect. When frost thickness increases further first a gradual and then a fast drop in capacity can be observed [2], and [5]. Both keep the fan speed constant during the experiments, thereby reflecting a conventional heat pump operating under frosting conditions. The capacity decrease occurs partly due to the insulating effect of the frost and mainly due to the blockage of the free flow area which leads to a strong decrease of the air flow rate followed by a drop in evaporation temperature and pressure as well as in COP.

1.2. Modeling of frost growth

Several models for predicting performance of finned tube heat exchangers under frosting conditions can be found in the open literature. Kondepudi and O'Neal [8] present a quasi-steady frost layer model taking the two mechanisms of increasing frost thickness and increasing frost density into account using a diffusion model to describe heat and mass transfer in the frost layer. Based on the reduction in the free flow area as frost grows the pressure drop over the coil is calculated. Seker [9] applies Kondepudi's model on a fin-and-tube geometry using various heat transfer and pressure drop correlations to include geometrical effects. An adaption to the original model is provided by Yao *et al.* [10] who treats the water vapor at the frost surface as ideal gas to derive an advanced equation for the frost density increase. Yang *et al.* [11] models frost growing on the tube and on the fin surface separately using a simplified water vapor diffusion equation. An additional dimension is added by Tso *et al.* [12] who uses the original model approach of Kondepudi and O'Neal and takes variations of frost thickness along the fins into account. A lumped parameter model is developed by Xia and Jacobi [13] to predict the performance of folded louvered fin heat exchangers. The mass flow of freezing water vapor attributing to the densification of the frost is accounted for by a constant absorption factor. In the frost layer only heat conduction is considered to calculate the frost surface temperature based on the exact solution to steady state heat conduction in a frosted fin between two flat tubes. Frost surface density is calculated based on that frost surface temperature. Experimentally derived curves for air side heat transfer coefficients and time dependent Reynolds number are used to compare the model with experimental data.

1.3. Defrosting

To operate a heat pump continuously under frost conditions at a certain point a defrost of the evaporator is necessary. For reversible air conditioners which are also used as heat pumps typically a reverse cycle defrost is initiated. During the defrost period the COP is negative due to the heat removal on the indoor side. Ideally the reverse cycle is terminated immediately after the frost has completely melted, but it is not trivial to detect this condition due to the uneven frost build-up.

Other typical defrost methods are electric resistance heating and hot gas bypass. All defrost methods have the common disadvantage of seriously penalizing the overall heat pump efficiency because they use energy while not delivering heating capacity during defrost. The more efficient methods of utilizing the refrigerant cycle for defrosting have the additional disadvantage of producing both thermal and pressure related stress on the unit in the switching transient. Optimization of the air source heat pump operation by determining the optimal defrost initiation condition, defrost operation time and intervals between defrosts has therefore attracted a significant research effort. One approach to prolong the time between defrosts is proposed by Mei *et al.* [14] who test a heat pump with an electric heater in the accumulator to allow for an overfeeding of the evaporator and thereby increasing evaporation

temperatures which will lead to prolonged intervals between defrost periods. Evaporator overfeeding might also reduce maldistribution problems which lead to further reduced evaporation temperatures as shown by Shao *et al.* [15]. Kwak and Bai [16] investigate a setup to fully avoid frost growth for small units by preheating the air at the evaporator inlet electrically a method however not yet tested on systems featuring active defrosting methods.

An alternative method to prolong the frost growth period is proposed in this paper which is based on shutting or cycling off individual circuits of a multicircuit evaporator. While the other circuits are operating normally no refrigerant is fed to the closed circuit, the circuit surface temperature rises due to the air passing the circuit and thus a passive defrost occurs. The objective of this paper is to illustrate generic system level effects of the chosen defrost schedule based by means of numeric simulations and to present experimental results showing the feasibility of the method.

2. The proposed defrost method

By using a new distributing valve (EcoFlow) as illustrated in Fig. 1 control of the flow of refrigerant through the different circuits is made possible. This is achieved by rotating the left disc shown in Fig. 1 such that refrigerant is pulsed through one valve outlet at a time. The desired distribution is specified in form of a distribution vector and is implemented as a dwell fraction in front of each outlet. The valve is equipped with control electronics that include a superheat control and a modbus interface. As discussed by Mader and Thybo [17] with this valve air and refrigerant maldistribution can be counteracted and hence the superheat zones equalized to better utilize the evaporator and therefore improve system efficiency.

The defrost off-cycling is achieved by specifying a distribution vector with zero dwell-time for the off-cycled circuit. The operational principle with the rotating upper disc is not able to close off the zero-dwell time circuit completely because it has to pass the hole opening. The minimum time passing the off-cycled circuit is 20 ms, which is equivalent to less than 0.5% of the nominal capacity. Hence, in the following it will be regarded as zero. The nominal rotation time of the upper disc is 10 s, so a given circuits is fed each 10 s. While operating with significantly larger off-cycling times in the defrost schedule it seems fair to disregard the disc rotational time in the defrost operation.

While the other circuits are operating normally no refrigerant is fed to the off-cycled circuit. Since the air continues to flow over the closed circuit the surface temperature rises and for air temperatures above 0 °C the frost melts and evaporates. For air temperatures below the freezing point the flow of the air leads to a compacting of the frost layer; thereby heat transfer is increased and capacity can be partly recovered. This principle is a normal feature in supermarket systems which is known to allow for a delay of the regular defrost and hence improve the system efficiency. Fig. 2 illustrates the overall cycle period for an evaporator with four circuits. Each circuit is alternately cycled off, this cycling is continuously performed under frosting conditions. Under light frost conditions it is possible to have all circuits running between two off periods.

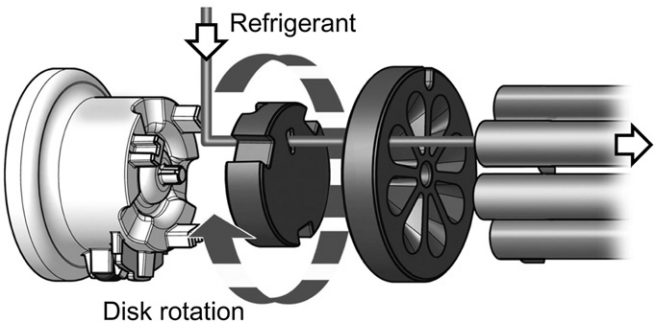

Fig. 1. The internal parts of the EcoFlow valve showing the distribution of refrigerant to the individual evaporator circuits.

3. Modeling

The objective of this paper is to illustrate generic system level effects of the chosen defrost schedule. For this purpose a considerably simplified quasi-steady mathematical model is derived for the frost growth period assuming an equal temperature and frost distribution throughout the evaporator.

The total refrigerant mass flow rate through the evaporator is calculated with a constant volume flow rate representing a constant compressor speed and the refrigerant density at saturation at evaporation temperature:

$$\dot{M}_{r,t} = \rho_r \dot{V} \tag{1}$$

The total mass flow rate is the sum of the individual mass flow rates through each circuit:

$$\dot{M}_{r,t} = \sum \dot{M}_r \tag{2}$$

The heat flow rate of an individual circuit is calculated with the individual refrigerant mass flow rate and the enthalpy difference between inlet and outlet:

$$\dot{Q} = \dot{M}_r (h_{rO} - h_{rI}) \tag{3}$$

The outlet enthalpy is the refrigerant enthalpy of saturated vapor at evaporation temperature, assuming each circuit mass flow is controlled such that saturated gas occurs at the outlet. The inlet enthalpy is constant and equal for each circuit, assuming no maldistribution of inlet quality.

On the air side the heat flow rate can be divided into sensible and latent heat:

$$\dot{Q} = \dot{Q}_s + \dot{Q}_l \tag{4}$$

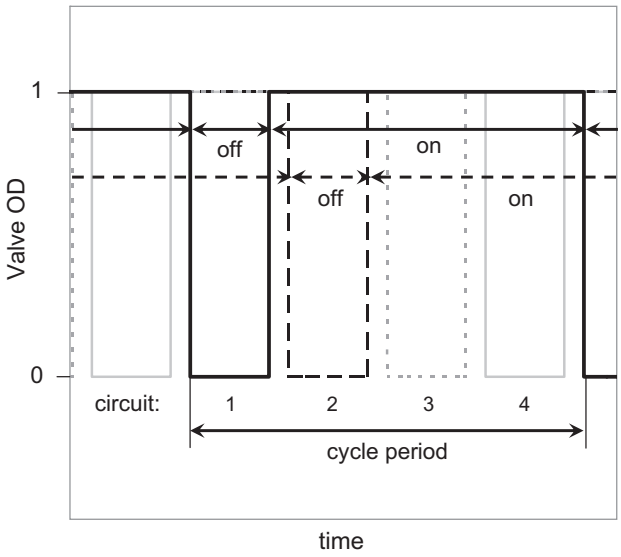

Fig. 2. Silent defrost algorithm: On and off cycling for four evaporator circuits.

Since the refrigerant temperature T_r is constant along the flow path it is assumed that also the temperature at the frost surface is constant throughout the evaporator. With this assumption an ε-NTU approach can be chosen to describe the sensible heat flow rate:

$$\dot{Q}_s = \dot{M}_a c_{p_a} \left[1 - e^{\left(\frac{-\alpha_a A_a}{\dot{M}_a c_{p_a}} \right)} \right] (T_{aI} - T_S) \tag{5}$$

Under the assumption of a constant frost surface temperature throughout the evaporator it can be reasoned that the humidity ratio X_S at the frost surface is also constant. Using the analogy of heat and mass transfer, a mass transfer efficiency can be defined similar to the heat transfer efficiency for that case and following equation for the mass flow rate of water to the evaporator surface can be deduced:

$$\dot{M}_f = \dot{M}_a \left[1 - e^{\left(\frac{-\beta A_a \rho_a}{\dot{M}_a} \right)} \right] (X_I - X_S) \tag{6}$$

The humidity ratio at the frost surface is assumed to be that of saturated humid air, the mass transfer coefficient β can be calculated from the heat transfer coefficient from Eq. (12) when for reasons of simplicity the Lewis number is assumed to be 1:

$$\beta = \frac{-\alpha_a}{\rho_a c_{p_a}} \tag{7}$$

The latent heat flow rate is finally calculated with the mass flow rate of water freezing at the evaporator surface and the enthalpy change from water vapor to ice Δh_f.

$$\dot{Q}_l = \dot{M}_f \Delta h_f \tag{8}$$

Neglecting the heat transfer resistance of the tube wall and resistance as well as vapor diffusion in the frost layer the evaporation temperature of the refrigerant T_r can be calculated using the total amount of heat transferred from refrigerant to the frost layer surface:

$$\dot{Q} = \alpha_r A_r (T_S - T_r) \tag{9}$$

The thickness of the frost layer is calculated using a constant frost density:

$$d_f = \frac{M_f}{\rho_f A_a}; \tag{10}$$

To describe the reduction of the cross flow area, the relative free cross flow area $\tilde{A} = A/A_0$ is introduced. It is assumed that the geometry between two tubes and two fins can be described as a rectangle, where the frost layer grows at the sides:

$$\tilde{A} = \frac{\left(H_{fin} - 2d_f \right) \left(P_{fin} - 2d_f \right)}{H_{fin} P_{fin}} \tag{11}$$

The reduction of the cross flow area reduces the heat transfer coefficient of the air side and also, since the fan speed is typically kept constant, the mass flow rate of air through the evaporator. Xia *et al.* [7] showed that the relation between Jason-Colburn factor and frost thickness for microchannel heat exchangers of different geometries can be described with polynomials which vary only slightly with differences in fin pitch and also with different air inlet conditions. Correlations for heat exchangers with round tubes and different fin geometry can be expected to differ. To calculate the actual mass flow rate for a certain frosting state typically a pressure drop model is applied taking into account the area decrease and combined either with a fan curve or with a plenum method where a virtual fixed air volume is treated as ideal gas. However as shown by Xia and Jacobi [13] the variation of friction factors with increasing frost layer thickness is extremely sensitive towards small changes in the fin geometry. Beside experimental data suffer from dramatic uncertainties for heavily frosted evaporators challenging the modeling and the accuracy of model predictions. For want of unambiguous pressure drop and heat transfer correlations for frosted heat exchangers the model instead describes the reduction of heat transfer coefficient and air mass flow rate with simple functions of the reduced area $\tilde{A}$.

$$\frac{\alpha_a}{\alpha_{a0}} = e^{(-2.5(1-\tilde{A}))} \tag{12}$$

$$\frac{\dot{M}_a}{\dot{M}_{a0}} = 1 - 0.06\left(1 - \tilde{A}\right) - 0.94\left(1 - \tilde{A}\right)^2 \tag{13}$$

The air side heat transfer coefficient for a clean coil α_{a0} as well as the refrigerant side heat transfer coefficient and the coefficients of the polynomial of Eq. (13) are fitted to experimental data for frost growth on a fin and tube evaporator. The curve to fit the coefficients is the one for 81% humidity shown in Fig. 3. The model then is able to reasonably predict both initial capacity and the capacity drop for a test run with an increased humidity of 86% for the same refrigerant volume flow rate and fan speed.

Transient models for a reversed cycle hot gas defrost are presented amongst others in Dopazo *et al.* [18] and Liu *et al.* [19], however to the knowledge of the authors there are no models describing a passive defrost by air blowing over the evaporator coil. Hence for modeling the defrosting period here only some basic assumptions are formulated.

In the defrost period after closing the valve the liquid refrigerant remaining in the circuit evaporates. The time until the circuit is evacuated depends on the mass of liquid refrigerant at the time of closing, the suction pressure and the heat transfer rate. During this time the frost layer continues to grow. As soon as all liquid refrigerant has evaporated, the temperature of the circuit and the frost

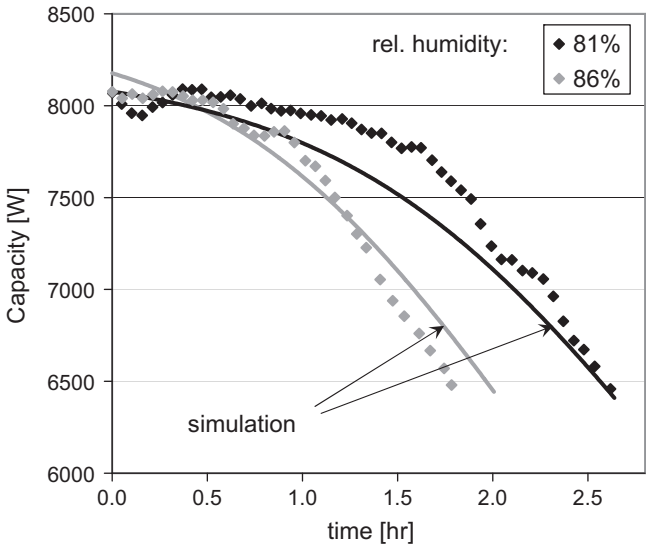

Fig. 3. Frost growth model validation on fin and tube evaporator.

starts to increase until it reaches the temperature of the inlet air. This whole period is modeled as a constant during which the transferred heat decreases linearly to zero and the frost surface temperature increases accordingly to the air inlet temperature. As soon as the humidity ratio at the frost surface exceeds the inlet humidity ratio, water starts to sublimate from the frost layer surface, this sublimation mass flow rate $\dot{M}_{f,s}$ can again be described by Eq. (6). A second process of frost removal starts as soon as the frost temperature increases beyond the freezing temperature and the frost starts to melt. The liquid then starts to drain both under the influence of gravity and the shear stress of air flowing over the surface. To maintain the model as simple as possible, again a correlation between the drainage mass flow rate $\dot{M}_{f,d}$ and the cross flow area of the evaporator is formulated using a factor F to adjust to experimental results:

$$\dot{M}_{f,d} = Fe^{(-2.5(1-d\tilde{A}))} \tag{14}$$

4. Simulation results illustrating optimality considerations

The on/off operation of one of the evaporator circuits while executing the silent defrost scheme is illustrated in Fig. 4. The circuit inlet is closed at $t = 720$ s, the opening degree of the valve is set to zero. The liquid refrigerant remaining in the circuit is evaporated during the initial part of the off-cycle period. Frost continues to grow, decreasing further the relative free cross flow area depicted as ratio $\tilde{A}$ for this circuit. When the surface temperature increases subsequently, the residual frost formation starts melting, $\tilde{A}$ starts to increase. Assuming the off-cycle period is long enough, the residual frost formation on the off-cycled evaporator circuit is totally melted, that part of the coil becomes frost free and $\tilde{A}$ equals one. The figure illustrates an off-cycle period that exceeds the melting period. Obviously, it is ideal to switch the circuit on just after the residual frost has been fully melted. Applying a shorter off-cycle time however causes a residual frost layer to remain on the coil for the next on period of the cycle. This will lead to a slow frost build-up of the coil until a reverse cycle defrost is eventually needed.

Two parameters can be adjusted to optimize the performance of the heat pump under this defrost operation scheme: The cycle period as illustrated in Fig. 2 and the defrost ratio which describes the ratio between the sum of all off-periods in a cycle to the total cycle period. For a defrost ratio of one, single circuits are switched off one after the other with no time in between where all circuits are fed; a defrost ratio of zero describes normal operation without cycling off of circuits. The choice of cycle period and defrost ratio therefore depends both on the evaporator geometry and the operating conditions. Different fin spacing, circuit number and inner volume of the evaporator require different settings. As described in the introductory part the frost growth depends on air temperature, humidity and velocity and coil surface temperatures. These conditions however also influence the frost melting efficiency in the off period of a circuit, making the adjustment of cycle period and defrost ratio necessary if an optimal performance should be reached.

Fig. 5 illustrates the changes in capacity over time for different defrost ratios. Shown is the time period until under normal operation the capacity is reduced by 20% compared to the clean coil and a defrost would be necessary. For a defrost ratio of one the time averaged capacity in the beginning of the frost growth period is below that of normal operation. This is caused by the fact that the total heat transfer area of the evaporator is reduced while a circuit is cycled off, resulting in lower evaporation temperatures and therefore lower capacities for a clean coil. While however under normal operation frost is continuously growing and the capacity drops, with the proposed defrost algorithm in operation the frost is melted regularly off the individual circuits, frost layers stay thin, a regular defrost is not necessary. Averaged over the whole time period, the capacity as well as the COP (illustrated in Fig. 6) is higher than under normal operation. A reduced defrost ratio of 0.6 leads to initially higher evaporation temperatures and therefore slower frost growth. However the off period of an individual cycle is too short to fully defrost the surface, frost is increasingly growing. The time until a regular defrost is necessary is nonetheless still delayed compared to the normal operation. For a defrost ratio of 0.2 the capacity is below that of normal operation during the whole period. Evaporation temperatures are only slightly reduced, the off period of an individual circuit is however shorter that the time needed to evaporate the liquid refrigerant in the circuit, no defrosting occurs. Fig. 6 depicts COP as well as relative air side cross flow area averaged over normal operating time until defrost. The COP as well as the free flow area is reduced for small defrost ratios compared to normal operation with a defrost ratio of zero until the circuit off periods are long enough

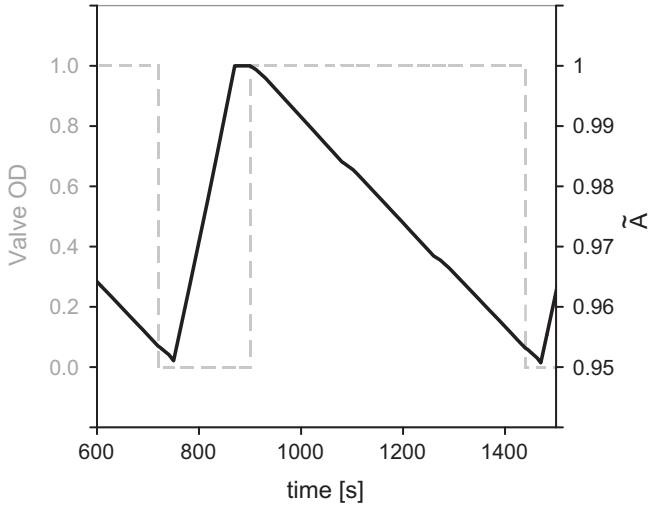

Fig. 4. Air side free flow area on one circuit.

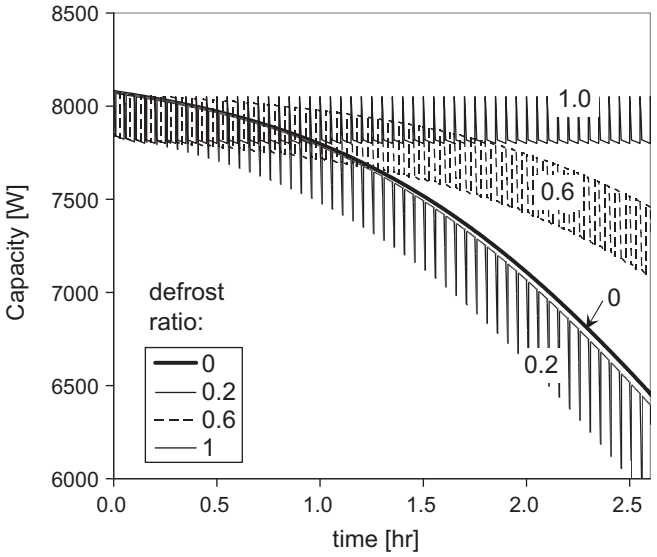

Fig. 5. Influence of defrost ratio on capacity during operation.

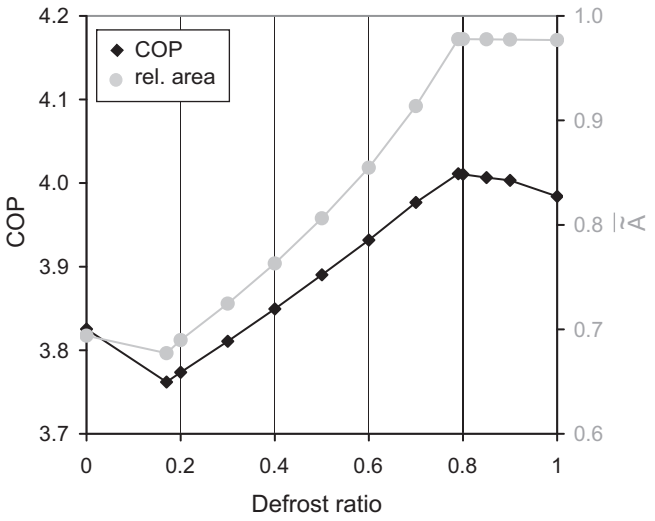

Fig. 6. Influence of defrost ratio on COP and relative cross flow area (both time averaged for operation until defrost.

to allow for the start of defrosting. With increasing defrost ratios the COP continuously increases, reaching a maximum for a ratio which ends the off period immediately when the circuit is totally frost free. Further increasing the defrost ratio does obviously not increase the averaged free flow area but reduces evaporation temperatures, causing the COP to drop again.

Similar observations can be made for varying cycle periods. Fig. 7 shows the maximum COP for varying cycle periods, each attained with the optimal defrost ratio. Too low cycle periods leave after evaporation of the remaining refrigerant too little time to perform a defrost, longer cycle periods lead to a stronger frost growth on the circuits in the on period, reducing the defrost efficiency due to a strongly decreased air flow through the coil.

Generally speaking long off-periods improve defrost of the off-cycled circuit however reduce evaporation temperatures and allow in the meantime for thicker frost layers to build on the remaining circuits hampering defrost efficiency due to reduced air flow. With an optimal choice of cycle period and defrost ratio a maximum in capacity and COP can be reached, for ambient air temperatures above the freezing point of water a regular defrost becomes superfluous. However also for non-optimal operation of the defrost algorithm under most operating conditions the number of regular defrosts can be reduced and therefore an increase of overall performance is gained. A special case is the operation under air temperatures below the freezing point of water. While for low air temperatures also the air humidity is lower and therefore frost growth is reduced, regular defrosts are typically still necessary. When operating the proposed defrost algorithm under these conditions during the off period the temperature of the circuit and the frost layer can not be increased above the melting point, only the mechanism of sublimation may reduce the frost. However from supermarket systems it is known that the structure of the frost changes towards denser frost layers. This reduces both the insulating effect of the frost layer and increases air side cross flow area, hence the periods between regular defrosts can also be increased for ambient air temperatures below the freezing point of water.

5. Experimental results

In the experimental setup a reversible residential air conditioning unit with a nominal cooling capacity of 10.5 kW is used. The split system consists of an indoor heat exchanger installed in an air duct and an outdoor heat exchanger which is operated as evaporator in heating mode. The outdoor heat exchanger is a louvered fin microchannel heat exchanger. In the inlet header baffles are inserted in a way that a number of parallel flat tubes comprise one circuit as schematically illustrated in Fig. 9a). The heat exchanger is divided into six such circuits in total.

The test procedure follows the AHRI Standard 210/240 [20] for heating mode test conditions for units having a variable speed compressor. Frost and defrost behavior is tested at intermediate compressor speed with an indoor temperature of 21.1 °C and an outdoor temperature of 1.67 °C with a relative humidity of 81.8%. Accuracy of the measurements follow the values given by the standard. Comparisons are made between a setup with a thermostatic expansion valve (TXV) mounted on the outdoor heat exchanger and one with the distributing valve, both are tested under the same operating conditions. Due to the possibility of balancing the refrigerant mass flow in the different circuits with the distributing valve the superheat at the outlet of the heat exchanger

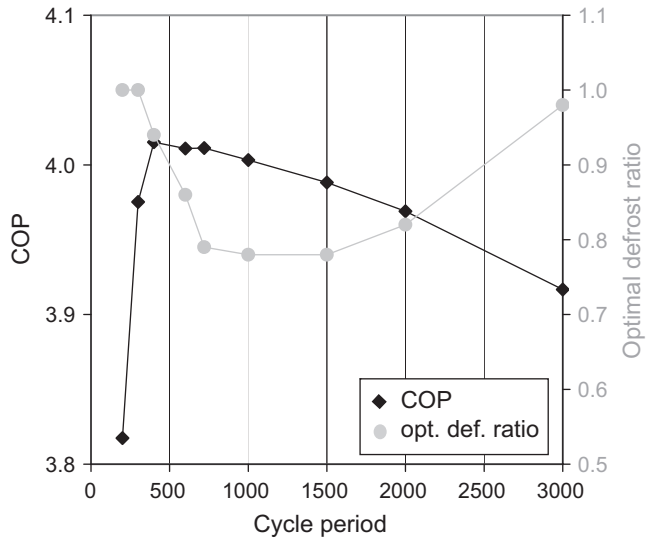

Fig. 7. Influence of cycle period.

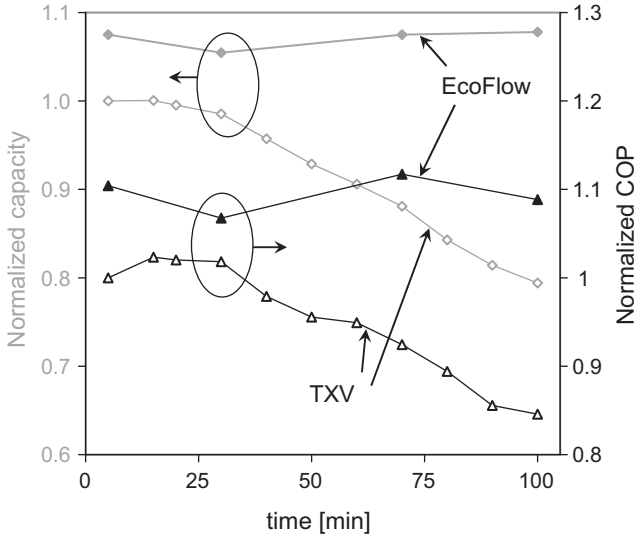

Fig. 8. Normalized capacity and COP for a heat pump with microchannel heat exchangers.

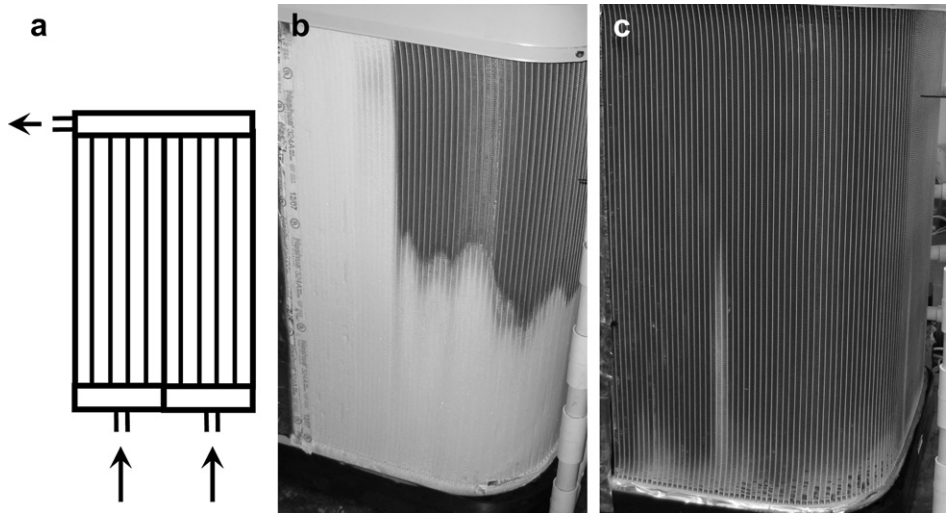

Fig. 9. Microchannel evaporator: Schematic illustration (a) and frost build up after 100 min operation with TXV (b) and distributing valve (c).

could be reduced to 3 K compared to 5 K for the TXV maintaining a stable superheat control. Since the outdoor heat exchanger is designed for cooling purposes mainly it is oversized for heating mode; hence the evaporation temperature could be increased by 2 K accordingly when operating the system with the distributing valve.

With the TXV tests are run until the capacity is dropped by 20% from the initial value which occurs at approximately 100 min operation time. Average values for capacity and COP are calculated for this period only, the impact of regular defrost is not taken into account for the comparisons made here. For the setup with the distributing valve a cycle period of 360 s with a defrost ratio of one is chosen. As Fig. 8 illustrates with the EcoFlow valve performing the on/off cycling of the circuits a continuous operation can be maintained without a drop in capacity or COP. After 100 min operation time at the end of each circuit off period the respective circuit is still fully defrosted. A visual comparison of the frost state at that time is given in Fig. 9b) and c) for operation with a TXV and the distributing valve respectively. Already at the frost free state with the EcoFlow valve an increase both in COP and capacity can be observed. This can partly be explained by the increase in evaporation temperature gained by reduced superheat temperatures. However also an increase in heat transfer coefficients with higher refrigerant velocities might play a role when only a part of the heat exchanger is in operation. The main effect leading to an improvement in system efficiency is however that strong build up of frost layers on the coil can be prevented under the given conditions. Averaged over 100 min operation time until a defrost would be necessary for the system with the TXV an increase in COP of approximately 15% can be achieved for the given system.

The tested microchannel heat exchanger is a prototype design with vertically oriented tubes. However also a horizontal orientation is possible. Previous tests showed that the distribution of liquid and gas phase in the header section is not affected by orientation: The momentum induced by the pulsation due to the rotation of the disk dominates the flow pattern. The defrost routine however needs adaptations in case of a horizontal orientation of the circuits. For evaporator geometries with round tubes and plate fins it was observed that circuits in the lower part of the heat exchanger have to be cycled off for longer periods than circuits in the upper part since some of the melted frost flows downwards and freezes on the lower circuits. This should be equally valid for microchannel geometries.

6. Conclusions

A new method of defrosting heat pump evaporators by cycling off individual evaporator circuits is presented. Based on a simple mathematical model the principles of the method as well as optimality considerations for adjusting the parameters of cycle time and defrost ratio are discussed in-depth. The feasibility of the method and the potential for improving system efficiency is demonstrated on an experimental setup with a microchannel heat exchanger in a system using variable capacity control. Comparing two similarly sized systems utilizing either a microchannel or a fin and tube evaporator Shao *et al.* [15] found that the system with a microchannel evaporator needs to operate with much shorter frosting periods both due to maldistribution effects and reduced fin spacing. The continuous frost removal of the proposed method prolongs the frosting period notably and therefore reduces the number of necessary standard defrosts or makes them even superfluous under many operating conditions. Hence the proposed method might be especially suitable for microchannel evaporators, though other tests not presented here were also conducted successfully for fin and tube geometries. The method requires to equip the system with a new type of valve and to adjust the parameters for the control routine. The evaporator circuitry for microchannel heat exchangers has to be adapted by sectioning the inlet header. Round tube with plate fin geometries can either be used directly without changes or the circuitry can be optimized for operation with the new defrost routine. No other changes in component design or system setup are necessary.

References

[1] K.-S. Lee, W.-S. Kim, KSME International Journal 13 (1999) 973–981.
[2] S. Tassou, C. Marquand, Applied Energy Volume 28 (1987) 19–33.
[3] P. Votsis, S. Tassou, D. Wilson, C. Marquand, Heat Recovery Systems and CHP 9 (1989) 399–406.
[4] W.-M. Yan, H.-Y. Li, Y.-J. Wu, J.-Y. Lin, W.-R. Chang, International Journal of Heat and Mass Transfer 46 (2003) 871–877.
[5] X.-M. Guo, Y.-G. Chen, W.-H. Wang, C.-Z. Chen, Applied Thermal Engineering 28 (2008) 2267–2278.
[6] S.N. Kondepudi, D.L. O'Neal, International Journal of Refrigeration 12 (1989) 151–158.
[7] Y. Xia, Y. Zhong, P. Hrnjak, A. Jacobi, International Journal of Refrigeration 29 (2006) 1066–1079.
[8] S.N. Kondepudi, D.L. O'Neal, International Journal of Refrigeration 16 (1993) 175–180.
[9] D. Seker, H. Karatas, N. Egrican, International Journal of Refrigeration 27 (2004) 367–374.

[10] Y. Yao, Y. Jiang, S. Deng, Z. Ma, International Journal of Heat and Mass Transfer 47 (2004) 3745–3756.
[11] D.-K. Yang, K.-S. Lee, S. Song, International Journal of Heat and Mass Transfer 49 (2006) 2619–2625.
[12] C. Tso, Y. Cheng, A. Lai, Applied Thermal Engineering 26 (2006) 111–120.
[13] Y. Xia, A. Jacobi, International Journal of Refrigeration 33 (2010) 321–333.
[14] V.C. Mei, R.E. Domitrovic, F.C. Chen, J.K. Kilpatrick, ASHRAE Transactions 108 (2002).
[15] L.-L. Shao, L. Yang, C.-L. Zhang, Applied Energy 87 (2010) 1187–1197.
[16] K. Kwak, C. Bai, Applied Thermal Engineering 30 (2010) 539–543.
[17] G. Mader, C. Thybo, DKV-Tagung Magdeburg (2010).
[18] J.A. Dopazo, J. Fernandez-Seara, F.J. . Uha, R. Diz, International Journal of Refrigeration 33 (2010) 829–839.
[19] Z. Liu, G. Tang, F. Zhao, Applied Thermal Engineering 23 (2003) 675–685.
[20] AHRI Standard 210/240-Performance Rating of Unitary Air-Conditioning & Air-Source Heat Pump Equipment (2008).